Sustainable Energy & Fuels

PAPER

View Article Online
View Journal | View Issue

Cite this: *Sustainable Energy Fuels*, 2018, **2**, 294

Silver bismuth iodides in various compositions as potential Pb-free light absorbers for hybrid solar cells†

Ki Woo Jung,[a] Mi Rae Sohn,[a] Hye Min Lee,[a] In Seok Yang,[a] Sang Do Sung,[a] Jeongho Kim,*[a] Eric Wei-Guang Diau[b] and Wan In Lee*[a]

Received 2nd October 2017
Accepted 6th November 2017

DOI: 10.1039/c7se00477j

rsc.li/sustainable-energy

Polycrystalline silver bismuth iodide (SBI) powders of various compositions (Ag : Bi = 2 : 1–1 : 1 in atomic ratio) were synthesized *via* a solid-state reaction in an evacuated Pyrex tube. Regardless of the composition of Ag and Bi, Ag_2BiI_5 in the hexagonal phase was preferentially formed and BiI_3 impurity in the rhombohedral phase was formed with the increase of the Bi component. The synthesized SBI powders of various compositions were applied as light absorbers for hybrid solar cells (HSCs), which employ mesoporous TiO_2 as the electron transporting layer and pristine spiro-OMeTAD as the hole transporting layer. To deposit light absorber layers, the coating solutions were prepared by dissolving the synthesized SBI powders in DMSO/DMF/HI and spin-coated over the mesoporous TiO_2 layer. For the solar cell employing pure Ag_2BiI_5, a photovoltaic conversion efficiency (PCE) of 1.74% was achieved, whereas the inclusion of the BiI_3 impurities in the Ag_2BiI_5 phase significantly increased the device performance. The highest PCE of 2.31% was achieved with the SBI of Ag : Bi = 55 : 45. Furthermore, the SBI solar cells show no hysteresis in the *J–V* curve measurements and are highly stable under ambient conditions, exhibiting excellent long-term stability at a relative humidity of 50%.

Introduction

All-solid-state hybrid solar cells (HSCs), consisting of a thin light absorber layer, a mesoporous inorganic electron transporting layer (ETL), and an organic hole transporting layer (HTL), have been diversely investigated over the last decade.[1–10] In particular, perovskite solar cells (PSCs), which employ methylammonium lead halide ($CH_3NH_3PbX_3$, X = I, Br or Cl) in the perovskite structure, have attracted great interest as next generation solar cells primarily due to their remarkable photovoltaic conversion efficiency (PCE) over 20%.[11–18] Among several methylammonium lead halides, $CH_3NH_3PbI_3$ is an excellent light absorber with a bandgap (1.55 eV) appropriate for utilization of solar light, a high molar absorption coefficient, extremely low exciton binding energy, an abnormally long charge diffusion length, and others. Moreover, $CH_3NH_3PbI_3$-based PSCs are much cheaper to fabricate than typical silicon solar cells, because the major components constituting the PSC devices are cheap and core parts of the device can be fabricated by a simple wet-chemical process.[16–19] Also, processes for large-area fabrication as well as flexible devices are now under development.[20–26] However, for the commercial application of PSC devices, several obstacles still need be overcome. Especially, Pb contained in perovskite light absorbers is a harmful element to our environment and has to be replaced by environmentally benign elements. Also, the poor stability of Pb-containing perovskite materials has to be overcome. Thus, it is important to develop Pb-free light absorbers with extended stability for the commercialization of PSC devices in the near future.

As a Pb-free light absorber, Sn-based perovskite materials have often been investigated.[27–32] By replacing Pb^{2+} with Sn^{2+}, $CH_3NH_3SnI_3$ can be synthesized by a simple solution process under inert conditions. $CH_3NH_3SnI_3$ has a narrower bandgap (1.23 eV) than $CH_3NH_3PbI_3$, which is more advantageous for utilizing the solar spectrum.[32] Thus far, a PCE over 6% has been achieved,[32] but $CH_3NH_3SnI_3$ has even poorer stability than $CH_3NH_3PbI_3$ because Sn^{2+} contained in $CH_3NH_3SnI_3$ is readily oxidized to Sn^{4+} under ambient conditions. Recently, Bi- and Sb-based light absorbers such as $(CH_3NH_3)_3Bi_2I_9$,[33–35] $(CH_3NH_3)_3Sb_2I_9$,[36] $Cs_3Sb_2I_9$ (ref. 37) and others were also investigated because Sb and Bi are much less harmful than Pb and the light absorbers containing these elements have excellent molar absorption coefficients of the order of 10^5 cm^{-1}. However, HSCs employing the light absorbers containing Bi or Sb exhibited photovoltaic conversion efficiencies (PCEs) of only less than

[a]*Department of Chemistry and Chemical Engineering, Inha University, Incheon 22212, Korea. E-mail: wanin@inha.ac.kr; jkim5@inha.ac.kr*

[b]*Department of Applied Chemistry, Institute of Molecular Science, National Chiao Tung University, Hsinchu 30010, Taiwan*

† Electronic supplementary information (ESI) available: Supplementary SEM images and *J–V* curves of solar cell devices are included. See DOI: 10.1039/c7se00477j

0.5% in most cases, except Zhang *et al.*'s recent report (PCE = 1.64%).[35] The reason for such low PCEs has not been clearly understood yet, but high exciton binding energy of those materials as well as difficulty of morphology control for their films might be responsible for the low PCE.[36,37] Double perovskite-type Cs_2AgBiX_6 (X = Br, Cl) structures were also investigated, but their band gaps turned out to be too large for application in light absorbers and significant photovoltaic performances were not acquired.[38–40] Mathews *et al.* studied the series of $(CH_3NH_3)_2CuCl_xBr_{4-x}$, belonging to 2-dimensional copper perovskite, but the achieved PCE from $(CH_3NH_3)_2CuCl_2Br_2$ was only 0.017%.[41]

Recently, silver-bismuth halides have been investigated as a potential light absorber for solar cells.[42–47] Sargent *et al.* prepared $AgBi_2I_7$ in the cubic phase with a bandgap of 1.87 eV, and achieved a PCE of 1.22% by applying it as a light absorber of HSCs.[45] Johansson *et al.* prepared Ag_2BiI_5 in the hexagonal phase with the bandgap of 1.85 eV, and reported a PCE of 2.1%.[46] Very recently, Turkevych *et al.* prepared silver-bismuth iodides of various compositions by a solid-state reaction in an evacuated silica tube at 600 °C.[47] Among them, Ag_3BiI_6 in the *R*3*m* rudorffite structure with the bandgap of 1.79–1.83 eV was reported to be the most efficient material for light absorbers. The fabricated FTO/mesoporous TiO_2/Ag_3BiI_6/PTAA/Au solar cell showed a noticeable PCE of 4.3%. The obtained results suggest that silver-bismuth halide materials can be a potential candidate for Pb-free light absorbers of perovskite solar cells. Furthermore, silver-bismuth halides offer significantly better stability than methylamine lead halides because they are not hygroscopic under ambient conditions.

In this work, we synthesized various silver bismuth iodides (SBIs) in the composition range of Ag : Bi = 2 : 1–1 : 1 by a solid-state reaction at 500 °C. Regardless of the composition in this range, Ag_2BiI_5 in the hexagonal phase was preferentially formed, whereas the $AgBiI_4$ phase was not formed at all. Instead, the rhombohedral BiI_3 phase was included in addition to the Ag_2BiI_5 phase. The obtained result suggests that the Ag_2BiI_5 phase is the most stable one among the SBI phases formed in the composition range of Ag : Bi = 2 : 1–1 : 1. We also found that the PSC devices employing the SBI with excess Bi showed significantly higher cell performance compared to those employing pure Ag_2BiI_5. We optimized the composition of SBI and discussed the role of the BiI_3 impurity phase mixed with Ag_2BiI_5 in enhancing the cell performance.

Results and discussion

Polycrystalline silver bismuth iodide (SBI) powders in the composition range of Ag : Bi = 2 : 1–1 : 1 were prepared *via* a solid-state reaction in an evacuated Pyrex tube. Fig. 1a shows the XRD patterns of SBI powders with the Ag-to-Bi molar ratios of 67 : 33, 60 : 40, 55 : 45, and 50 : 50. In spite of the compositional variation in this range, the Ag_2BiI_5 in the hexagonal phase (ICDD cards 00-023-1025) was the main phase for all of the synthesized powders. The pure Ag_2BiI_5 phase was formed from the AgI and BiI_3 powders mixed with a molar ratio of 67 : 33 (SBI-67 : 33). When the Ag to Bi ratio was 60 : 40, the BiI_3 peaks

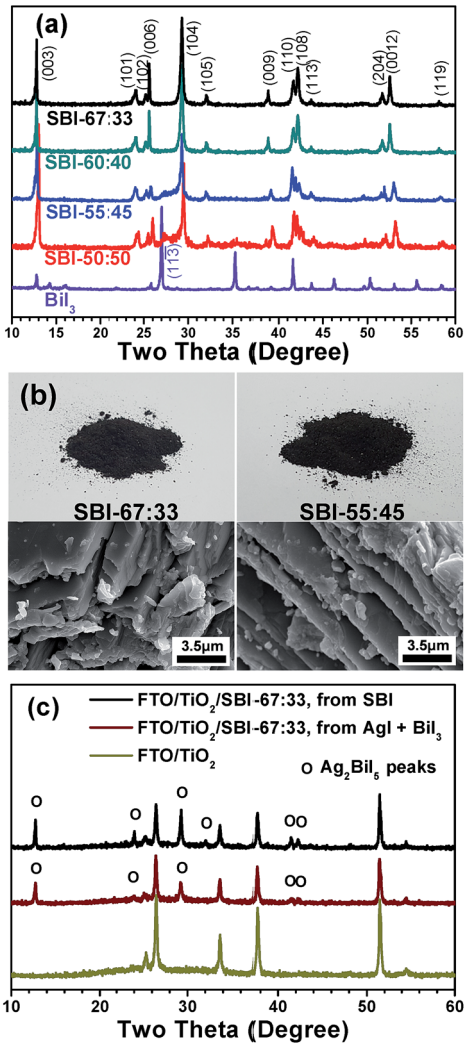

Fig. 1 XRD patterns of the polycrystalline SBI powders in various Ag to Bi molar ratios prepared by a solid-state reaction at 500 °C and the BiI_3 powder in the rhombohedral phase (a), photographic and SEM images of Ag_2BiI_5 (SBI-67 : 33) and SBI-55 : 45 powders (b), and XRD patterns of the Ag_2BiI_5 films deposited on the FTO/TiO_2 by the coating solutions of Ag_2BiI_5 powder and the mixture of AgI and BiI_3, respectively (c). XRD patterns of the bare FTO/TiO_2 substrate are also included.

were not observed by XRD analysis within the detection limit, but noticeable BiI_3 diffraction peaks were detected for the SBI in the composition of 55 : 45 (SBI-55 : 45). That is, an additional peak at 26.98° is identified to be the $(11\bar{3})$ peak of the rhombohedral BiI_3 phase (ICDD cards 00-007-0269). In the SBI samples prepared with the Ag-to-Bi molar ratio of 50 : 50 (SBI-50 : 50), the intensity of the BiI_3 peak further increases, but the major component is still the hexagonal Ag_2BiI_5 phase, and the $AgBiI_4$ phase was not formed.[43] The obtained result is compatible with the phase diagrams of silver bismuth iodides reported by Babanly *et al.*[48] Fig. 1b shows the photographic and scanning electron microscopy (SEM) images of the as-prepared SBI-67 : 33 (pure Ag_2BiI_5) and SBI-55 : 45 powders. Both samples exhibit a blackish color, and the individual particles have a kind of plate-like structure.

For the formation of SBI films, the synthesized SBI powders were dissolved in a mixed solvent of DMF/DMSO/HI and the prepared solution was then spin-coated on the mesoporous TiO_2 layer, followed by heat treatment at 120 °C. The XRD patterns of the SBI-67 : 33 film, as shown in Fig. 1c, reveal that the film has the same crystallographic phase as the initial Ag_2BiI_5 powder. As a control experiment, a film was prepared from a simple mixture of AgI and BiI_3 with a molar ratio of 67 : 33, that is, without the SBI synthesis. The XRD patterns of the control film sample are also shown in Fig. 1c, showing that the diffraction peaks representing the Ag_2BiI_5 phase are not as intense as those of the film derived from the synthesized SBI powder. This result clearly indicates that the coating solution prepared from the SBI powders is much more effective in forming the highly crystallized phase in the fabricated film.

UV-visible absorption spectra were obtained for the SBI-67 : 33 (that is, pure Ag_2BiI_5) and SBI-55 : 45 films deposited on the mesoporous TiO_2 layer, as shown in Fig. 2a. The absorption spectra of these two films of the same thickness are quite similar to each other in the overall shape, but we reproducibly monitored that the SBI-55 : 45 film shows relatively higher absorbance. Compared with the $CH_3NH_3PbI_3$ film of the same thickness, these two films exhibit appreciably higher absorbance in the wavelength range of 550–650 nm, suggesting that the prepared SBI materials are well suited for harvesting the solar light. Details for the SBI-67 : 33, SBI-55 : 45 and $CH_3NH_3PbI_3$ films used for the measurement of the absorption spectra are described in Fig. S1.†

The absorption band edge of the SBI-67 : 33 and SBI-55 : 45 films was estimated to be ~680 nm, and their band gaps were determined to be 1.88 and 1.83 eV, respectively, according to the Tauc plots shown in Fig. 2b. On the other hand, the quantum yield of photoluminescence (PL) is very low for both SBI-67 : 33 and SBI-55 : 45 with their PL intensities estimated to be less than $1/10^5$ that of $CH_3NH_3PbI_3$. As a result, the dynamics of charge injection or recombination for SBI-67 : 33 and SBI-55 : 45 cannot be determined by conventional time-resolved PL techniques.

The valence band (VB) level of the as-prepared Ag_2BiI_5 layer coated on the TiO_2 layer was determined by ultraviolet photoelectron spectroscopy (UPS). As shown in Fig. 3a, the cutoff energy (E_{cutoff}) was 16.85 eV, leading to the Fermi level (E_F) of 4.37 eV from the equation, E_F = 21.22 eV (He I) − E_{cutoff}. Consequently, the VB level (E_{VB}) of Ag_2BiI_5 was determined to be −5.63 eV from the E_{VB} − E_F value of 1.26 eV obtained by the linear extrapolation in the low binding energy region of the UPS spectrum, as shown in the inset of Fig. 3a. As a result, the conduction band (CB) level of Ag_2BiI_5 was estimated to be −3.75 eV from its band gap of 1.88 eV, which was determined from the absorption spectrum (see Fig. 2b). Thus, the locations of the VB and CB of Ag_2BiI_5 are suitable for hybrid solar cells, employing typical ETL materials such as TiO_2 and SnO_2 and HTL materials such as spiro-OMeTAD and PTAA.[49–51] That is, in our solar cell devices, the electrons generated from the Ag_2BiI_5

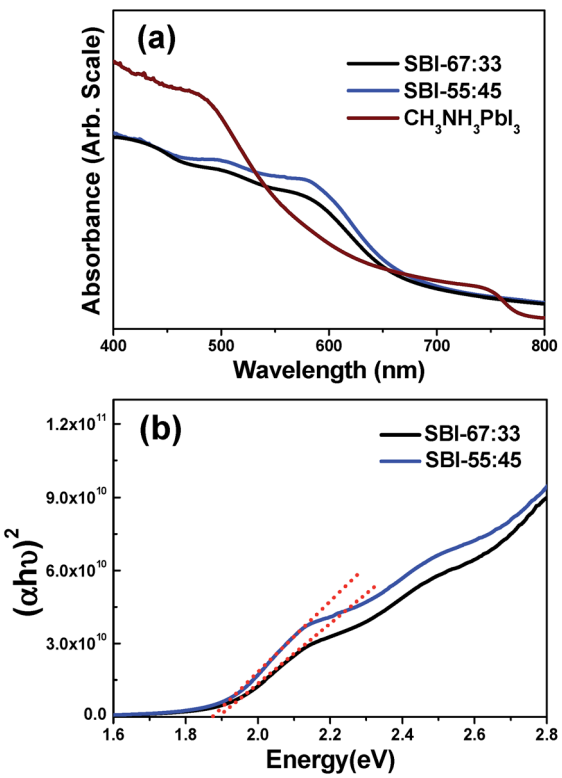

Fig. 2 Absorption spectra of Ag_2BiI_5, SBI-55 : 45, and $CH_3NH_3PbI_3$ films coated on the mesoporous TiO_2 layer (a), and Tauc plots of Ag_2BiI_5 and SBI-55 : 45 films (b). Thickness of each film over the mesoporous TiO_2 layer was controlled to ~60 nm for the comparison of absorbance.

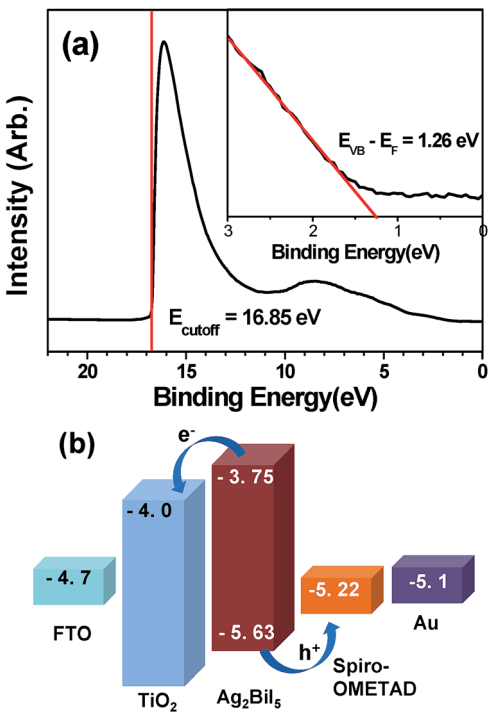

Fig. 3 UPS spectrum for the high binding-energy region of the Ag_2BiI_5 film coated on the mesoporous TiO_2 layer while its low-binding-energy region is shown in the inset (a), and the energy band diagram for charge separation occurring in the Ag_2BiI_5 solar cell (b).

can be efficiently injected into the CB of TiO_2, while the holes can move into the HOMO level of spiro-OMeTAD, as described in Fig. 3b. A similar behavior is expected for the SBI-55 : 45 because its major crystallographic phase is Ag_2BiI_5.

First of all, pure Ag_2BiI_5 was employed for the fabrication of solar cells. Ag_2BiI_5 solutions of various concentrations were prepared by dissolving stoichiometric amounts of the as-prepared pure Ag_2BiI_5 powders in DMF/DMSO/HI, and each solution was spin-coated on the mesoporous TiO_2 layer. The Ag_2BiI_5 will be deposited into the internal pores as well as overlay-coated on the mesoporous TiO_2 layer.

Fig. 4 illustrates plan-view and cross-sectional-view SEM images of the various Ag_2BiI_5 films prepared from the coating solutions of different concentrations. It was seen from the plan-view SEM images of Fig. 4a that, when the 0.2 M solution of Ag_2BiI_5 was employed as the coating solution, approximately 50% of the TiO_2 surface was covered with Ag_2BiI_5 grains and the remaining 50% of the TiO_2 surface seems to be exposed without the coverage of Ag_2BiI_5. When employing 0.3 M solution, about 80% of the TiO_2 surface is covered by Ag_2BiI_5. With 0.4 M solution, most of the TiO_2 surface is covered by Ag_2BiI_5 grains except for a few pinholes observed, whereas 0.5 M solution induces complete coverage of the TiO_2 surface with Ag_2BiI_5. From the cross-sectional-view SEM images in Fig. 4b, it can be seen that the thickness of the Ag_2BiI_5 layer on the TiO_2 surface increases to 30, 60, 100 and 150 nm as the concentration of the coating solution increases to 0.2, 0.3, 0.4 and 0.5 M respectively. Fig. 4c shows the cross-section of the fabricated Ag_2BiI_5 solar cell device with the configuration of FTO/TiO_2/Ag_2BiI_5/spiro-OMeTAD/Au. The thickness of the Ag_2BiI_5 layer, prepared from a 0.3 M solution, is ~60 nm, while the thicknesses of mesoporous TiO_2, spiro-OMeTAD and the Au counter electrode (CE) layer are ~220, 150, and 60 nm, respectively.

J–V curves were measured for the solar cell devices, which have the configuration of FTO/TiO_2/Ag_2BiI_5/spiro-OMeTAD/Au. Fig. 5a shows the *J–V* curves of the PSC devices employing the Ag_2BiI_5 layer with various thicknesses. Detailed photovoltaic parameters are listed in Table 1. The solar cell device employing the Ag_2BiI_5 layer coated with 0.2 M solution gives the PCE of 1.07%, while the device obtained from 0.3 M solution exhibits the PCE of 1.74%, which is the highest value among the Ag_2BiI_5-based devices. This result is rather unexpected because the mesoporous TiO_2 surface is only partially covered with the Ag_2BiI_5 layer in these devices. In contrast, the Ag_2BiI_5 films obtained from 0.4 M and 0.5 M solutions show relatively lower PCE values of 1.42 and 1.15%, respectively, although the surface of the TiO_2 layer is fully covered by Ag_2BiI_5 grains.

To achieve high device performance in hybrid solar cells, in principle, the light absorber layer has to cover the surface of the ETL uniformly and its thickness has to be optimized. That is, full coverage of the TiO_2 surface will be advantageous in reducing charge recombination between the electrons in the CB of TiO_2 and the holes in the HOMO of the HTM, because TiO_2 and the HTM are not in contact with each other in this case. Moreover, the light absorber layer needs to be thick enough to utilize the solar light effectively. In this work, however, the PCE values of the devices with the TiO_2 layer fully covered by Ag_2BiI_5 were significantly lower than those of the devices with the partially covered one. We believe that this observation is closely related to fast recombination between the separated electrons and holes in Ag_2BiI_5. If the Ag_2BiI_5 layer is thick, the electrons and holes generated in Ag_2BiI_5 have to travel long distances to arrive at TiO_2 and spiro-OMeTAD, respectively. Hence, charge recombination between electron–hole pairs can occur easily if the charge diffusion coefficients of Ag_2BiI_5 are small. In our experimental result, optimized photovoltaic performance was achieved with the Ag_2BiI_5 layer that partially covers the TiO_2 surface with a thickness of ~60 nm, clearly indicating that

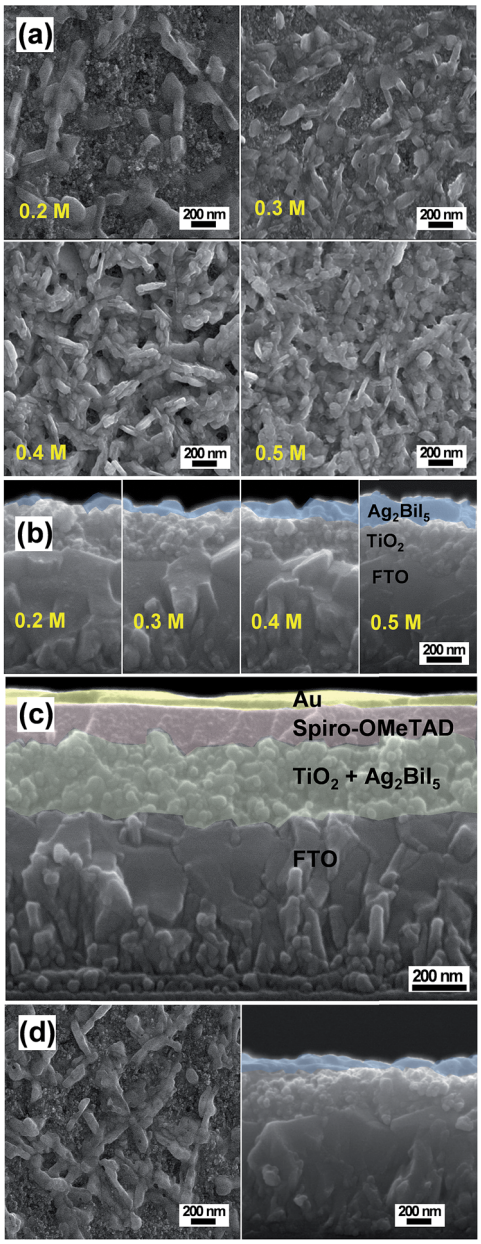

Fig. 4 Plan view (a) and cross-sectional view (b) SEM images of Ag_2BiI_5 layers prepared by the coating solutions of different concentrations, and cross-section of a typical solar cell device employing the Ag_2BiI_5 layers coated with 0.3 M solution (c). Plan-view and cross-sectional-view SEM images of the SBI 55 : 45 film coated with 0.3 M solution (d).

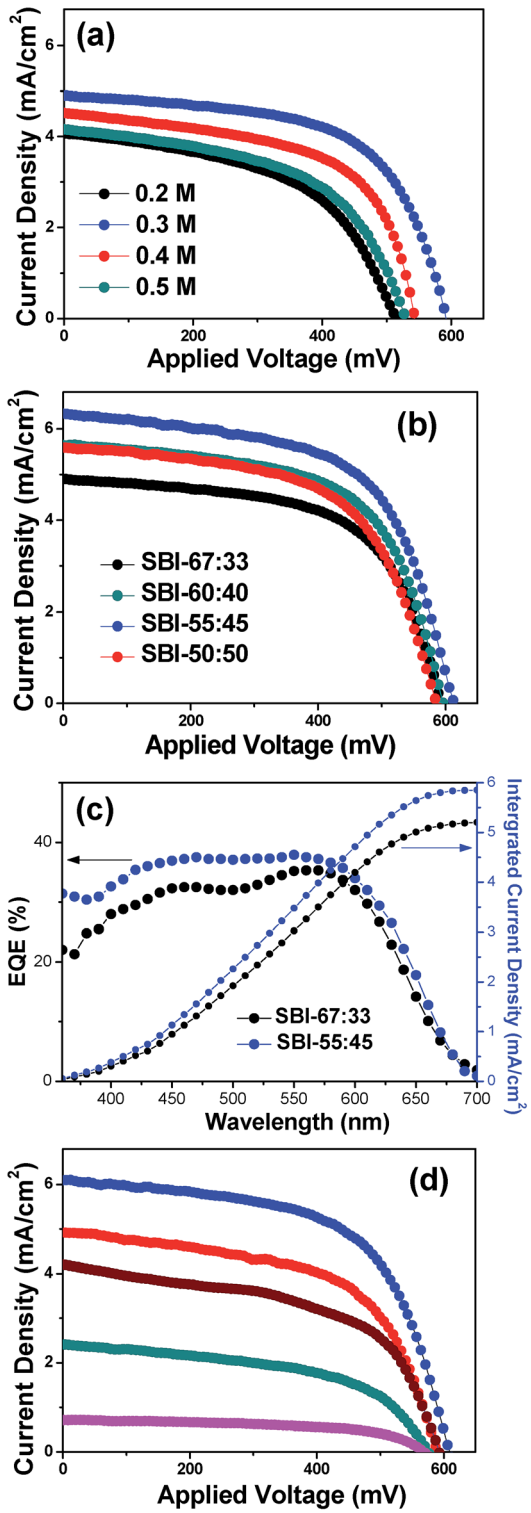

Fig. 5 J–V curves of the Ag_2BiI_5 solar cells employing various Ag_2BiI_5 layers derived from the coating solutions of different concentrations (a) and the solar cell devices employing the various SBI films in different Ag to Bi ratios. (b). IPCE spectra and integrated current densities for the optimized SC-Ag_2BiI_5 and SC-SBI-55 : 45 devices (c), and J–V curves of the SC-SBI-55 : 45 measured under various light intensities (1, 0.7, 0.5, 0.3 and 0.1 sun) (d).

intrinsically Ag_2BiI_5 has fast charge recombination properties. According to the energy band diagram shown in Fig. 3b, however, the V_{OC} of the Ag_2BiI_5-based solar cell is expected to be higher than 1 V, but the obtained V_{OC} value is only 592 mV. This also suggests that significant charge recombination occurs in these solar cell devices.

SBI samples of SBI-60 : 40, SBI-55 : 45 and SBI-50 : 50 were also applied as light absorbers for HSCs. For the coating of each SBI layer, 0.3 M solution was used and the solar cell devices of FTO/TiO_2/SBI/spiro-OMeTAD/Au were fabricated by employing the same process that was applied to the Ag_2BiI_5-based solar cell (SC-Ag_2BiI_5). Fig. 5b shows the J–V curves of the solar cell devices employing various SBI films. Notably, it was observed that the excess Bi component induces the enhancement of PCE. As a result, the device with SBI-55 : 45 (SC-SBI-55 : 45) exhibits the highest efficiency. However, the SBI-50 : 50 containing higher Bi component leads to relatively lower efficiency. SC-SBI-55 : 45 showed the optimum PCE of 2.31% with a V_{OC} of 614 mV, J_{SC} of 6.329 mA cm^{-2}, and FF of 59.34%. J_{SC} and V_{OC} values were significantly increased, whereas FF was not appreciably changed, compared to those of SC-Ag_2BiI_5. Presently, the role of the BiI_3 impurity phase in enhancing the cell efficiency is not clear, but higher light absorption of SBI-55 : 45 than that of SBI-67 : 33 is one of the major reasons for the increased J_{SC}. In addition, the inclusion of the BiI_3 impurity phase seems to be helpful for the electron and hole transport through the Ag_2BiI_5 layer to TiO_2 and Spiro-OMeTAD, respectively, which may cause retardation of charge recombination, thus increasing the V_{OC}.

IPCE spectra were obtained for the SC-Ag_2BiI_5 and SC-SBI-55 : 45, as shown in Fig. 5c. The J_{SC} values acquired from the integration of the IPCE spectra match the values acquired from the J–V curves in Fig. 5b. The external quantum efficiency (EQE) maxima for the solar cells with Ag_2BiI_5 and SBI-55 : 45 were 35% and 38% at the wavelength of 550 nm. Comparatively low EQE is ascribed to considerable charge recombination occurring in the device.

As shown in Fig. 5d, the J–V curves of the SC-SBI-55 : 45 were measured at the light intensities in the range of 0.1–1 sun. The maximum PCE of 2.74% was acquired under a light intensity of 0.5 sun. Detailed photovoltaic parameters are listed in Table 1. The obtained result suggests that the SBI-55 : 45 layer is too thin to completely utilize the photons irradiated from 1 sun. Hence, the amount of SBI-55 : 45 deposited on the TiO_2 layer has to be increased for the complete utilization of solar light. The same trend was also obtained for the SC-Ag_2BiI_5 devices, as shown in Fig. S2.†

As a control experiment, a 0.3 M SBI-55 : 45 coating solution was prepared by dissolving stoichiometric amounts of AgI and BiI_3 in the mixed solvent of DMF/DMSO/HI. To form the SBI-55 : 45 layer, the prepared solution was then spin-coated and heat-treated under the same conditions. Fig. S3† shows the J–V curves of the solar cell devices employing two different SBI-55 : 45 films, derived from the synthesized SBI-55 : 45 and the mixture of AgI and BiI_3, respectively. Herein, the device derived from the mixture of AgI and BiI_3 solution showed much poorer efficiency (PCE = 1.10%) with significantly lower J_{SC} and V_{OC} values. The obtained result clearly indicates that the

Table 1 Photovoltaic parameters of SBI-based solar cells fabricated and analyzed under different conditions. First, the concentrations of coating solution were varied in preparing the SBI-67 : 33 films. Second, the SBI films in various compositions were coated by using the 0.3 M solution. Third, the photovoltaic parameters of SC-SBI-55 : 45 were obtained under different light intensities. Fourth, PV parameters were obtained by reverse and forward voltage scans

Solar cells					
SBIs (Ag : Bi)	Preparation or measurement conditions	V_{OC} (mV)	J_{SC} (mA cm^{-2})	FF (%)	PCE (%)
67 : 33	0.2 M	515	4.075	51.13	1.07
	0.3 M	592	4.898	59.96	1.74
	0.4 M	543	4.518	57.94	1.42
	0.5 M	529	4.159	52.38	1.15
67 : 33	0.3 M	592	4.898	59.96	1.74
60 : 40		596	5.640	60.73	2.04
55 : 45		614	6.329	59.34	2.31
50 : 50		587	5.593	58.25	1.91
55 : 45	1 sun	612	6.116	59.21	2.22
	0.7 sun	590	4.917	57.97	2.40
	0.5 sun	594	4.206	54.84	2.74
	0.3 sun	576	2.413	51.33	2.38
	0.1 sun	569	0.710	54.72	2.21
55 : 45	Backward	614	6.329	59.34	2.31
	Forward	618	6.235	59.20	2.28
67 : 33	Backward	592	4.898	59.96	1.74
	Forward	593	4.876	59.82	1.73

employment of the SBI powders synthesized *via* a solid-state reaction induces superior photovoltaic performance, presumably due to considerably higher crystallinity in the fabricated SBI films (see Fig. 1c).

SBI-based solar cells are highly stable under ambient conditions, revealing excellent stability at a relative humidity of 50% at 25 °C. Fig. 6a shows the change of PCE as a function of aging time for the SC-SBI-55 : 45 and SC-SBI-67 : 33. Extended stability against aging under moisture is ascribed to the intrinsic properties of SBI materials without hygroscopicity. Furthermore, SC-SBI-55 : 45 as well as SC-SBI-67 : 33 show negligible hysteresis in the *J*–*V* curve measurements, as shown in Fig. 6b and Table 1. The PCE values for backward and forward scans were coincident within measurement error.

Regarding the stability and hysteresis, SBI-based solar cells have remarkable advantages. Although SBI-based solar cells in this work show a low cell performance, we expect that the PCE can be improved greatly in the near future, considering that their molar extinction coefficients are comparable to or even higher than $CH_3NH_3PbI_3$. For the enhancement of PCE in SC-SBI devices, first of all, charge extraction from the SBI layers has to be improved, because Ag_2BiI_5 and SBI-55 : 45 show a high rate of charge recombination. In this regard, appropriate materials for the ETL and HTL have to be developed, and the architectures of the ETL or HTL have to be designed for efficient charge collection. In addition, new coating techniques, which facilitate the control of the thickness and grain structure of the SBI layer as well as induce excellent step-coverage over the mesoporous ETL, have to be developed. The interface control at ETL/SBI and SBI/HTL will also be an important issue.

In addition, SBIs with bandgaps of 1.8–1.9 eV are considered to be an appropriate material for the construction of tandem solar cells with high efficiency. At present, GaInP is mainly employed in fabricating the top cell of tandem devices. For instance, the champion PCEs of 31.6% and 32.8% were reported

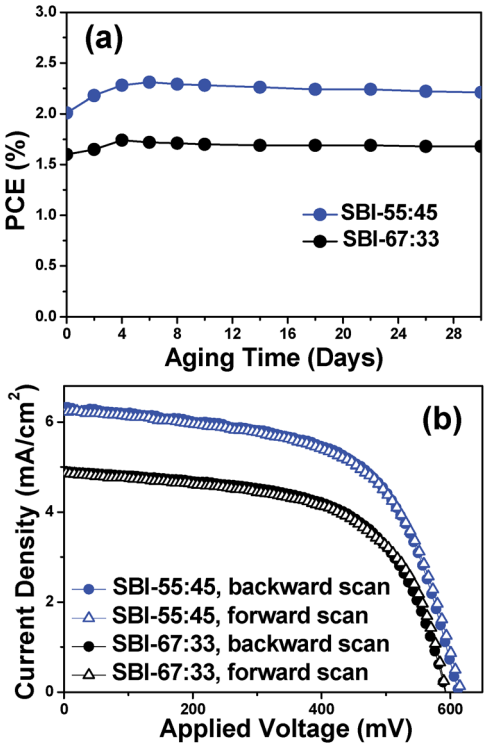

Fig. 6 PCE changes of SC-SBI-55 : 45 and SC-SBI-67 : 33 as a function of aging time at a relative humidity of 50% at 25 °C (a), and their *J*–*V* curves acquired by forward and backward scans at a scan rate of 100 mV s^{-1} (b).

from the tandem devices of GaInP/GaAs and GaInP/Si, respectively.[52–54] Considering that the band gaps of SBIs are very close to that of GaInP, SBI solar cells can be a potential candidate for the top cell of tandem devices in the future.

Experimental

Preparation of polycrystalline silver bismuth iodide (SBI) powders

0.1 mol BiI_3 (99%, Aldrich) and a stoichiometric amount of AgI (99.9%, Alfa) were mixed and ground for 30 min under an Ar environment. The mixed powder was then inserted into a Pyrex tube and evacuated for 2 h with a mechanical pump. The tube kept at 1.5 ± 0.5 mTorr was sealed using a torch, and subsequently annealed at 500 °C for 12 h. The collected silver bismuth iodide (SBI) powders with a blackish color were gently ground under an Ar environment.

Preparation of SBI coating solutions

First, the coating solutions for the SBI film were prepared by dissolving 0.3 g of the as-synthesized SBI powders in the solvent mixture of dimethyl sulfoxide (DMSO), dimethlyformamide (DMF) and HI (57% aqueous solution, Aldrich) with a volume ratio of 3 : 1 : 0.2. Particularly, solutions of 0.2, 0.3, 0.4, and 0.5 M concentrations were prepared by varying the amount of mixed solvent added. To obtain neat solutions, the solutions were magnetically stirred for 2 h.

Second, the coating solutions were prepared from the AgI and BiI_3 powders. That is, stoichiometric amounts of AgI and BiI_3 powders were dissolved in the mixed solvent of DMSO, DMF and HI (3 : 1 : 0.2 in volume). Typically, to obtain 0.3 M coating solution for Ag_2BiI_5 film, 0.141 g AgI, 0.157 g BiI_3, and 1.0 mL of the mixed solvent were mixed and stirred for 2 h.

Fabrication of SBI HSCs

The patterned FTO glass (Pilkington, TEC8) was dipped into 1 mM HCl solution for 5 min and washed with deionized water. As a TiO_2 compact layer, an ~10 nm thick Ti film was deposited using a RF magnetron sputtering system (A-Tech system, Korea), followed by oxidation at 500 °C for 30 min in air. A mesoporous TiO_2 layer with ~220 nm thickness was then spin-coated at 7000 rpm for 60 s using the TiO_2 paste, which was obtained by diluting the commercial TiO_2 paste (DyeSol 18NRT) by 1 : 6 in volume with the mixed solvent of terpineol and ethanol (2 : 3 in volume). The coated films were then heated at 500 °C for 30 min. The prepared TiO_2 layer was then dipped into 0.2 M $TiCl_4$ solution at 70 °C for 30 min, followed by annealing at 500 °C for 30 min.

Approximately 0.05 mL SBI coating solutions of various concentrations were then dropped onto the mesoporous TiO_2 layers. After a stay of 5 s, the films were spun at 4000 rpm for 20 s. To improve the uniformity of the film, 0.5 mL ether was dropped during the spinning. The coated films were then heated on a hot plate at 120 °C for 10 min. Pristine spiro-OMeTAD (2,2′,7,7′-tetrakis(*N*,*N*-bis(*p*-methoxyphenyl)amino)-9,9′-spirobifluorene) was used for the preparation of the HTL because the added additives can react with silver bismuth iodides, as illustrated in Fig. S4.† That is, the solution of 72.3 mg spiro-OMeTAD dissolved in 1.0 mL chlorobenzene without adding any additives was spin-coated at 4000 rpm for 30 s. For the back contact, the Au layer with a thickness of ~50 nm was deposited by using a thermal evaporator (Korea Vacuum Tech.).

Measurements and characterization

Photocurrent density–voltage (*J*–*V*) measurements were performed using a source measurement unit (Model 2400, Keithley). A solar simulator (Model K730, McScience) with AM 1.5G intensity was used as the light source and the light intensity was adjusted using an NREL-calibrated Si solar cell equipped with a KG-5 filter. The solar cell devices were masked with a non-reflective black metal aperture to define the active area, typically 0.122 cm^2, while the active area of each device was measured using an optical microscope. In the measurement of *J*–*V* curves, the scan rate was 100 mV s^{-1}, and the dwell time before the voltage scan was 20 s. Incident photon-to-current efficiency (IPCE) was measured as a function of wavelength from 300 nm to 800 nm using an IPCE system specially designed for dye-sensitized solar cells (PV Measurements, Inc.).

Conclusions

By a solid-state reaction of AgI and BiI_3 mixtures in the composition range of Ag : Bi = 2 : 1–1 : 1 at 500 °C, polycrystalline Ag_2BiI_5 powders in the hexagonal phase were preferentially formed with inclusion of the rhombohedral BiI_3 impurity phase. It was found that the presence of BiI_3 impurities in the Ag_2BiI_5 phase significantly increased the performance of SBI solar cells. The highest PCE of 2.31% was achieved from the SBI in the composition of Ag : Bi = 55 : 45, whereas the pure Ag_2BiI_5 induces only 1.74%. The higher light absorption of SBI-55 : 45 is considered to be a main reason for the increased J_{SC}. Moreover, the presence of the BiI_3 impurity phase may play a favorable role for charge separation in the Ag_2BiI_5 layer, leading to suppression of charge recombination. In addition, SBI layers derived from the SBI powders synthesized by a solid-state reaction exhibit better performance than those from the mixture of AgI and BiI_3 when they were applied as a light absorber layer of the solar cell devices. Furthermore, the fabricated devices reveal no hysteresis in the *J*–*V* curve measurements, and are highly stable under ambient conditions, exhibiting excellent long-term stability at a relative humidity of 50% at 25 °C.

Conflicts of interest

There are no conflicts to declare.

Acknowledgements

This work has been supported by the Ministry of Science, ICT and Future Planning (MSIP) through the National Research Foundation of Korea (NRF) (2015M1A2A2052999).

Notes and references

1 H. J. Snaith, S. M. Zakeeruddin, L. Schmidt-Mende Lukas, C. Klein and M. Grätzel, *Angew. Chem., Int. Ed.*, 2005, **44**, 6413–6417.
2 H. J. Snaith, A. J. Moule, C. Klein, K. Meerholz, R. H. Friend and M. Grätzel, *Nano Lett.*, 2007, **7**, 3372–3376.
3 A. Chang, S. H. Im, Y. H. Lee, H.-J. Kim, C.-S. Lim, J. H. Heo and S. I. Seok, *Nano Lett.*, 2012, **12**, 1863–1867.
4 H.-S. Kim, C.-R. Lee, J.-H. Im, K.-B. Lee, T. Moehl, A. Marchioro, S.-J. Moon, R. Humphry-Baker, J.-H. Yum, J. E. Moser, M. Grätzel and N.-G. Park, *Sci. Rep.*, 2012, **2**, 591.
5 M. M. Lee, J. Teuscher, T. Miyasaka, T. N. Murakami and H. J. Snaith, *Science*, 2012, **338**, 643–647.
6 J. H. Noh, S. H. Im, J. H. Heo, T. N. Mandal and S. I. Seok, *Nano Lett.*, 2013, **13**, 1764–1769.
7 J. Han, Z. Liu, K. Guo, J. Ya, Y. Zhao, X. Zhang, T. Hong and J. Liu, *ACS Appl. Mater. Interfaces*, 2014, **6**, 17119–17125.
8 X. Liu, J. Chen, M. Luo, M. Leng, Z. Xia, Y. Zhou, S. Qin, D.-J. Xue, L. Lv, H. Huang, D. Niu and J. Tang, *ACS Appl. Mater. Interfaces*, 2014, **6**, 10687–10695.
9 Y. Zhou, L. Wang, S. Chen, S. Qin, X. Liu, J. Chen, D.-J. Xue, M. Luo, Y. Cao, Y. Cheng, E. H. Sargent and J. Tang, *Nat. Photonics*, 2015, **9**, 409–415.
10 N. G. Park, *Mater. Today*, 2015, **18**, 65–72.
11 National Renewable Energy Laboratory, Solar Cell Efficiency Chart, http://www.nrel.gov/ncpv/images/efficiency_chart.jpg, accessed July 2016.
12 D. Bi, C. Yi, J. Luo, J. D. Décoppet, F. Zhang, S. M. Zakeeruddin, X. Li, A. Hagfeldt and M. Grätzel, *Nat. Energy*, 2016, **1**, 16142.
13 E. H. Anaraki, A. Kermanpur, L. Steier, K. Domanski, T. Matsui, W. Tress, M. Saliba, A. Abate, M. Grätzel, A. Hagfeldt and J. P. Correa-Baena, *Energy Environ. Sci.*, 2016, **9**, 3128–3134.
14 W. S. Yang, B.-W. Park, E. H. Jung, N. J. Jeon, Y. C. Kim, D. U. Lee, S. S. Shin, J. Seo, E. K. Kim, J. H. Noh and S. I. Seok, *Science*, 2017, **356**, 1376–1379.
15 H.-S. Kim, J.-Y. Seo and N.-G. Park, *ChemSusChem*, 2016, **9**, 2528–2540.
16 Z. Song, C. L. McElvany, A. B. Phillips, I. Celik, P. W. Krantz, S. C. Watthage, G. K. Liyanage, D. Apul and M. J. Heben, *Energy Environ. Sci.*, 2017, **10**, 1297–1305.
17 M. A. Green, A. Ho-Baillie and H. J. Snaith, *Nat. Photonics*, 2014, **8**, 506–514.
18 L. K. Ono, N.-G. Park, K. Zhu, W. Huang and Y. Qi, *ACS Energy Lett.*, 2017, **2**, 1749–1751.
19 X. Liu, F. Kong, R. Ghadari, S. Jin, T. Yu, W. Chen, G. Liu, Z. Tan, J. Chen and S. Dai, *Chem. Commun.*, 2017, **53**, 9558–9561.
20 I. Jeong, H. Jung, M. Park, J. S. Park, H. J. Son, J. Joo, J. Lee and M. J. Ko, *Nano Energy*, 2016, **28**, 380–389.
21 J. Yoon, H. Sung, G. Lee, W. Cho, N. Ahn, H. S. Jung and M. Choi, *Energy Environ. Sci.*, 2017, **10**, 337–345.
22 W. Chen, Y. Wu, Y. Yue, J. Liu, W. Zhang, X. Yang, H. Chen, E. Bi, I. Ashraful, M. Grätzel and L. Han, *Science*, 2015, **350**, 944–948.
23 K.-C. Wang, P.-S. Shen, M.-H. Li, S. Chen, M.-W. Lin, P. Chen and T.-F. Guo, *ACS Appl. Mater. Interfaces*, 2014, **6**, 11851–11858.
24 B. J. Kim, D. H. Kim, Y.-Y. Lee, H.-W. Shin, G. S. Han, J. S. Hong, K. Mahmood, T. K. Ahn, Y.-C. Joo, K. S. Hong, N.-G. Park, S. Lee and H. S. Jung, *Energy Environ. Sci.*, 2015, **8**, 916–921.
25 X. Xu, Q. Chen, Z. Hong, H. Zhou, Z. Liu, W.-H. Chang, P. Sun, H. Chen, N. D. Marco, M. Wang and Y. Yang, *Nano Lett.*, 2015, **15**, 6514–6520.
26 M. Park, H. J. Kim, I. Jeong, J. Lee, H. Lee, H. J. Son, D.-E. Kim and M. J. Ko, *Adv. Energy Mater.*, 2015, **5**, 1501406.
27 M. Konstantakou and T. Stergiopoulos, *J. Mater. Chem. A*, 2017, **5**, 11518–11549.
28 M. H. Kumar, S. Dharani, W. L. Leong, P. P. Boix, R. R. Prabhakar, T. Baikie, C. Shi, H. Ding, R. Ramesh, M. Asta, M. Grätzel, S. G. Mhaisalkar and N. Mathews, *Adv. Mater.*, 2014, **26**, 7122–7127.
29 T. M. Koh, T. Krishnamoorthy, N. Yantara, C. Shi, W. L. Leong, P. P. Boix, A. C. Grimsdale, S. G. Mhaisalkar and N. Mathews, *J. Mater. Chem. A*, 2015, **3**, 14996–15000.
30 F. Hao, C. C. Stoumpos, D. H. Cao, R. P. Chang and M. G. Kanatzidis, *Nat. Photonics*, 2014, **8**, 489–494.
31 Y. He and G. Galli, *Chem. Mater.*, 2014, **26**, 5394–5400.
32 N. K. Noel, S. D. Stranks, A. Abate, C. Wehrenfennig, S. Guarnera, A.-A. Haghighirad, A. Sadhanala, G. E. Eperon, S. K. Pathak, M. B. Johnston, A. Petrozza, L. M. Herza and H. J. Snaith, *Energy Environ. Sci.*, 2014, **7**, 3061–3068.
33 B. W. Park, B. Philippe, X. Zhang, H. Rensmo, G. Boschloo and E. M. J. Johansson, *Adv. Mater.*, 2015, **27**, 6806–6813.
34 T. Singh, A. Kulkarni, M. Ikegami and T. Miyasaka, *ACS Appl. Mater. Interfaces*, 2016, **8**, 14542–14547.
35 Z. Zhang, X. Li, X. Xia, Z. Wang, Z. Huang, B. Lei and Y. Gao, *J. Phys. Chem. Lett.*, 2017, **8**, 4300–4307.
36 J.-C. Hebig, I. Kühn, J. Flohre and T. Kirchartz, *ACS Energy Lett.*, 2016, **1**, 309–314.
37 B. Saparov, F. Hong, J.-P. Sun, H.-S. Duan, W. Meng, S. Cameron, I. G. Hill, Y. Yan and D. B. Mitzi, *Chem. Mater.*, 2015, **27**, 5622–5632.
38 E. T. McClure, M. R. Ball, W. Windl and P. M. Woodward, *Chem. Mater.*, 2016, **28**, 1348–1354.
39 M. R. Filip, S. Hillman, A. A. Haghighirad, H. J. Snaith and F. Giustino, *J. Phys. Chem. Lett.*, 2016, **7**, 2579–2585.
40 R. E. Brandt, V. Stevanovic, D. S. Ginley and T. Buonassisi, *MRS Commun.*, 2015, **5**, 265–275.
41 D. Cortecchia, H. A. Dewi, J. Yin, A. Bruno, S. Chen, T. Baikie, P. P. Boix, M. Grätzel, S. Mhaisalkar, C. Soci and N. Mathews, *Inorg. Chem.*, 2016, **55**, 1044–1052.
42 H. C. Sansom, G. F. Whitehead, M. S. Dyer, M. Zanella, T. D. Manning, M. J. Pitcher, T. J. Whittles, V. R. Dhanak, J. Alaria, J. B. Claridge and M. J. Rosseinsky, *Chem. Mater.*, 2017, **29**, 1538–1549.
43 Z. Xiao, W. Meng, D. B. Mitzi and Y. Yan, *J. Phys. Chem. Lett.*, 2016, **7**, 3903–3907.
44 A. H. Slavney, T. Hu, A. M. Lindenberg and H. I. Karunadasa, *J. Am. Chem. Soc.*, 2016, **138**, 2138–2141.

45 Y. Kim, Z. Yang, A. Jain, O. Voznyy, G. H. Kim, M. Liu, L. N. Quan, F. P. García de Arquer, R. Comin, J. Z. Fan and E. H. Sargent, *Angew. Chem., Int. Ed.*, 2016, **55**, 9586–9590.
46 H. Zhu, M. Pan, M. B. Johansson and E. M. J. Johansson, *ChemSusChem*, 2017, **10**, 2592–2596.
47 I. Turkevych, S. Kazaoui, E. Ito, T. Urano, K. Yamada, H. Tomiyasu, H. Yamagishi, M. Kondo and S. Aramaki, *ChemSusChem*, 2017, **10**, 3754–3759.
48 L. F. Mashadieva, Z. S. Aliev, A. V. Shevelkov and M. B. Babanly, *J. Alloys Compd.*, 2013, **551**, 512–520.
49 N. Ahn, D.-Y. Son, I.-H. Jang, S. M. Kang, M. Choi and N.-G. Park, *J. Am. Chem. Soc.*, 2015, **137**, 8696–8699.
50 N. J. Jeon, J. H. Noh, Y. C. Kim, W. S. Yang, S. Ryu and S. I. Seok, *Nat. Mater.*, 2014, **13**, 897–903.
51 C. Bi, Q. Wang, Y. Shao, Y. Yuan, Z. Xiao and J. Huang, *Nat. Commun.*, 2015, **6**, 7747.
52 S. Essig, C. Allebé, T. Remo, J. F. Geisz, M. A. Steiner, K. Horowitz, L. Barraud, J. S. Ward, M. Schnabel, A. Descoeudres, D. L. Young, M. Woodhouse, M. Despeisse, C. Ballif and A. Tamboli, *Nat. Energy*, 2017, **2**, 17144.
53 B. M. Kayes, L. Zhang, R. Twist, I.-K. Ding and G. S. Higashi, *IEEE J. Photovoltaics*, 2014, **4**, 729–733.
54 J. J. Berry, J. van de Lagemaat, M. M. Al-Jassim, S. Kurtz, Y. Yan and K. Zhu, *ACS Energy Lett.*, 2017, **2**, 2540–2544.